

GEOLOGIC MAPPING OF THE SCHRÖDINGER BASIN AREA, LUNAR SOUTH POLE. S.C. Mest^{1,2} and L.E. Van Arsdall³, ¹Planetary Science Institute, 1700 E. Ft. Lowell, Suite 106, Tucson, AZ 85719-2395 (mest@psi.edu) at ²Planetary Geodynamics Laboratory (Code 698), NASA GSFC, Greenbelt, MD 20771; ³Dept. of Geology and Environmental Geosciences, College of Charleston, 66 George St., Charleston, SC 29424-0001.

Introduction: In this study we use high resolution Clementine images and topographic data to map the geology and geomorphology of a 90 degree quadrangle near the lunar south pole. This study is part of a larger effort to map the south polar region (Lq30) to 60° S at 1:2.5M scale [1,2] in accordance with the USGS' Lunar Geologic Mapping Program [<http://astrogeology.usgs.gov/Projects/PlanetaryMapping/Lunar/>].

The south pole has been identified as a high-priority target for future exploration and is of interest because of the postulated occurrence of perennial ice in permanently shadowed areas. Our scientific motivation concerns characterization of the south polar terrain, which could be supplied to mission planners and integrated into analyses to assess potential landing sites.

Previous Work: Wilhelms et al. [3] provide the most detailed mapping effort of this area, which is Lunar Orbiter-based and mapped at 1:5M scale. More recent mapping of the floor of Schrödinger basin [4], based on preliminary Clementine data, shows more detail than [3], but was done prior to acquisition of Lunar Prospector data, and therefore does not include NS and GRS data. Recent mapping of Shackleton crater [5] using Arecibo radar and SMART-1 AMIE images found that Shackleton formed ~3.6 bya, nearly 300 my older than previous estimates [3]. Our goal is to update the lunar map resource by incorporating the most recent and most complete datasets available, primarily Clementine and Lunar Prospector.

Background: This study covers a 90 degree quadrant (90-180°) on the lunar far-side extending from the south pole to 70° S and is part of Lunar Quadrangle Lq30. This quadrant is located within the South Pole-Aitken Basin, the oldest (pre-Nectarian), deepest (~12 km), and largest (~2600 km) lunar basin [6-9]. It is believed the SPA impact event may have excavated down to the lower crust, which Clementine and Lunar Prospector remote sensing data confirms by the enrichment of FeO and Th [e.g., 10-13], making the floor of SPA geologically unique on the moon. This quadrant includes two large multi-ring impact basins, the pre-Nectarian-aged Amundsen-Ganswindt basin (D=335 km; 81°S, 120°E) and the Imbrian-aged Schrödinger basin (D=312 km; 76°S, 134°E), and presumably much of the surface materials consist of their ejecta as well as ejecta from other nearby basins.

Methodology: This project utilizes ArcGIS (v. 9.2) to prepare map layers (e.g., image mosaics, topography, spectral maps) and conduct the mapping, which fol-

lows the work of [14] in their mapping of the Copernicus Quadrangle (Lq11). The Clementine UV-VIS 750-nm mosaic (100 m/pixel) is being used as the primary base to characterize geologic units from surface textures and albedos, identify unit contacts, and identify impact craters with diameters greater than 2 km; other mosaics and images (e.g., Lunar Orbiter, Clementine NIR) are being used as well. The convenience of GIS software for mapping of this scale (~1:2.5M) is that multiple layers - units, structures, contacts, spectral, and shaded relief - can be georeferenced to display different characteristics about a zone of interest while, at the same time, large scale trends can be observed.

Results: Here we describe the geologic materials identified in the map area [1,2] (Fig. 1) and we present regional crater size-frequency distribution results (Fig. 2) for this quadrant.

Geologic materials: Seventeen units have been identified and are organized into three groups: Highland Materials, Crater Materials, and Schrödinger Materials.

Highland Materials are believed to predate or coincide with formation of the Amundsen-Ganswindt and Schrödinger Basin-forming events and are likely some of the oldest materials in this area (Fig. 1). These materials form elevated terrains, sequences of ridges and depressions, and most intercrater highland surfaces.

Crater Materials are found throughout the map area and include material emplaced by impact events or by subsequent mass wasting of impact materials (Fig. 1); many of these deposits are gradational, making identification of their parent crater difficult. Other members of this group include materials that mantle craters or are found along the walls or floors of craters.

Schrödinger Materials, particularly the floor materials, appear to form some of the youngest deposits in this quadrant (Fig. 1). Most of Schrödinger's floor deposits show smooth surfaces degraded to varying amounts and display lobate edges. The eastern part of Schrödinger contains a well-preserved ovoidal depression interpreted to be the source of at least two pyroclastic eruptions [4]. Most of the floor exhibits broad flat expanses of rough material that fills low-relief areas. Based on albedos and surface textures, as well as the abundance of intersecting fissures throughout Schrödinger, our interpretations for these materials are in agreement with previous authors [e.g., 2-4] in that the Schrödinger floor materials are indicative of effusive fissure eruptions followed by pyroclastic eruptions centered at the ovoidal depression.

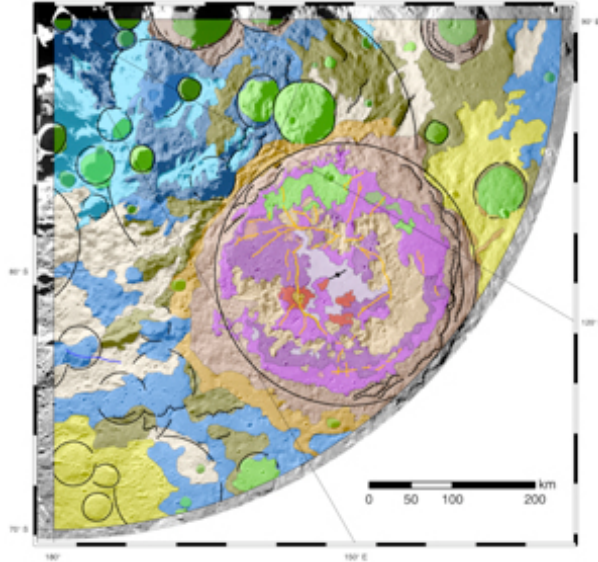


Figure 1. Preliminary geologic map of the Schrödinger quadrant (60°-90°S, 90°-180°E) within Lq30. Shown are Schrödinger Materials (red, purple and brown polygons), Crater Materials (yellow, green and olive polygons), and Highland Materials (blue and beige polygons); orange lines within Schrödinger are fractures.

Crater Size-Frequency Distributions: All impact craters with $D > 2$ km have been identified in the Schrödinger quadrant. In this study we are principally interested in statistical representations of the entire population as a standard for age-dating of discrete units. However, classifying by crater type - primary or secondary - has a significant effect on our results. The effect is considered noteworthy because an overwhelming number of secondary craters steepen the SFD curve [15] (Fig. 2). However, a secondary advantage to this error is that ascertaining the slope gradient (or 'cross-over diameter') is often used to derive unit-specific age-constraints. Where high-resolution image data allowed, craters were classified as either secondary or primary. Secondary craters were identified by their tendency to be found in clusters, chains, and their amorphous shape, whereas primaries were identified by their pristine, symmetrical, and singular occurrence. The classification as primary or secondary is treated here as a statistical experiment to determine if any meaningful correlations exist between secondary versus primary distribution and unit ages. For the purposes of overall age determination however, we use both primary and secondary craters to derive SFDs.

Figure 2 shows SFD results for the Schrödinger quadrant. Compared to the Hartmann isochrons, the quadrant clearly shows a pre-Nectarian to Nectarian age for the total crater population (green circles). At small diameters (< 7 km), the Primary curve (red circles) is shallower than the Secondary curve (blue circles) but follows the total population at $D > 7$ km.

Conclusions: This mapping effort is in the process of upgrading the lunar map record for the south pole and here we present the map of the Schrödinger Basin area. We have mapped at higher resolution using ArcGIS software to produce a more detailed, more accurate, and more informative map than its predecessors. Contacts have been mapped in increased detail and in places revised from previous efforts. Albedo and surface texture, the key factors in unit identification and description, are more readily discernible than previous maps [3]. This map has the capacity to be used in mission planning; our hope is that future missions will be able to use our results as a staging ground for potential moon-landings.

Ongoing Work: This research is preliminary and will continue to refine geologic contacts and unit interpretations. Once mapping is concluded, crater size-frequency distributions will be calculated for each unit identified to place them in stratigraphic context.

References: [1] Mest, S.C. (2007) LPSC XXXVIII, Abs. #1842. [2] Van Arsdall, L.E. and S.C. Mest (2008), LPSC XXXIX, Abs. #1706. [3] Wilhelms, D.E., et al. (1979) *Geologic map of the south side of the Moon*, U.S.G.S. Misc. Inves. Ser. Map I-1162, 1:5M scale. [4] Shoemaker, E.M., et al. (1994) *Science*, **266**, 1851-1854. [5] Spudis, P.D. et al. (2008) LPSC XXXIX, Abs. #1626. [6] Wilhelms, D.E (1987) *The Geologic History of the Moon*, U.S. Geol. Survey Prof. Pap. **1348**. [7] Spudis, P.D. (1993) *The Geology of Multi-Ring Impact Basins*, 263 pp. [8] Spudis, P.D. et al. (1994) *Science*, **266**, 1848-1851. [9] Zuber, M.T. et al. (1994) *Science*, **266**, 1839-1843. [10] Pieters, C.M., et al. (1997) *GRL*, **24**, 1903-1906. [11] Lawrence, D.J., et al. (1998) *Science*, **281**, 1484-1489. [12] Lucey, P.G., et al. (1998) *JGR*, **103**, 3701-3708. [13] Jolliff, B.L., et al. (2000) *JGR*, **105**, 4197-4216. [14] Gaddis, L.R., et al. (2005) LPSC XXXVIII, Abs. #2021. [15] McEwen, A. S. and E.B. Bierhaus (2006) *Annual Rev. Earth and Planet. Sci.*, **34**, 535-567.

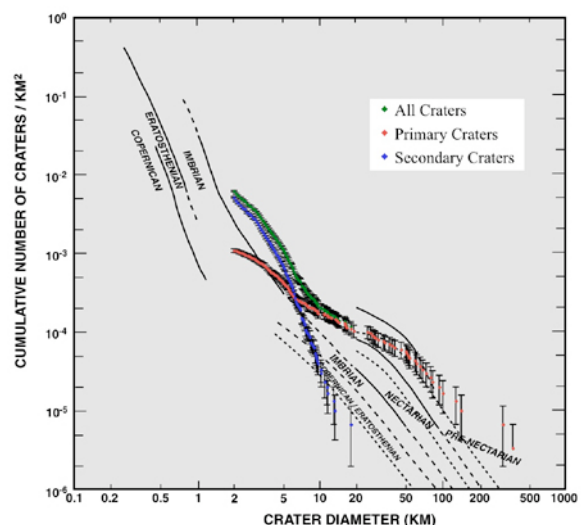


Figure 2. Regional crater size-frequency distributions for the Schrödinger quadrant (60°-90°S, 90°-180°E).